HHS Public Access

Author manuscript

Biochemistry. Author manuscript; available in PMC 2021 April 07.

Published in final edited form as:

Biochemistry. 2020 April 07; 59(13): 1338–1350. doi:10.1021/acs.biochem.0c00047.

Structural Features of an Extended C-Terminal Tail Modulate the Function of the Chemokine CCL21

Natasha A. Moussouras,
Department of Microbiology & Immunology, Medical College of Wisconsin, Milwaukee, Wisconsin 53226, United States

Gertrud M. Hjortø,
Department of Biomedical Sciences, University of Copenhagen, Copenhagen 2200, Denmark

Francis C. Peterson
Department of Biochemistry, Medical College of Wisconsin, Milwaukee, Wisconsin 53226, United States

Martyna Szpakowska, **Andy Chevigné**
Department of Infection and Immunity, Immuno-Pharmacology and Interactomics, Luxembourg Institute of Health, Esch-sur-Alzette L-4354, Luxembourg

Mette M. Rosenkilde,
Department of Biomedical Sciences, University of Copenhagen, Copenhagen 2200, Denmark;

Brian F. Volkman,
Department of Biochemistry, Medical College of Wisconsin, Milwaukee, Wisconsin 53226, United States;

Michael B. Dwinell
Department of Microbiology & Immunology, Medical College of Wisconsin, Milwaukee, Wisconsin 53226, United States;

Abstract

The chemokines CCL21 and CCL19, through binding of their cognate receptor CCR7, orchestrate lymph node homing of dendritic cells and naïve T cells. CCL21 differs from CCL19 via an unstructured 32 residue C-terminal domain. Previously described roles for the CCL21 C-terminus include GAG-binding, spatial localization to lymphatic vessels, and autoinhibitory modulation of

Corresponding Authors: bvolkman@mcw.edu, mdwinell@mcw.edu.

Supporting Information

The Supporting Information is available free of charge at https://pubs.acs.org/doi/10.1021/acs.biochem.0c00047.
Full 15N–^{1}H HSQC overlays of dilution series for CCL21WT; full 15N–^{1}H HSQC overlays of dilution series for CCL21trunc; effects of CCL21WT and CCL21trunc on cell chemotaxis; heteronuclear-NOE (hetNOE) results for CCL21 C80AC99A; residues 80–90 responsible for the structural differences between CCL21WT and CCL21trunc (PDF)

Accession Codes

Human CCL21, UniProtKB: O00585.

Complete contact information is available at: https://pubs.acs.org/10.1021/acs.biochem.0c00047

The authors declare the following competing financial interest(s): B.F.V., M.B.D., and F.C.P. are co-founders and have ownership interests in Protein Foundry, LLC.

CCR7-mediated chemotaxis. While truncation of the C-terminal tail induced chemical shift changes in the folded chemokine domain, the structural basis for its influence on CCL21 function remains largely unexplored. CCL21 concentration-dependent NMR chemical shifts revealed weak, nonphysiological self-association that mimics the truncation of the C-terminal tail. We generated a series of C-terminal truncation variants to dissect the C-terminus influence on CCL21 structure and receptor activation. Using NMR spectroscopy, we found that CCL21 residues 80–90 mediate contacts with the chemokine domain. In cell-based assays for CCR7 and ACKR4 activation, we also found that residues 92–100 reduced CCL21 potency in calcium flux, cAMP inhibition, and β-arrestin recruitment. Taken together, these structure–function studies support a model wherein intramolecular interactions with specific residues of the flexible C-terminus stabilize a less active monomer conformation of the CCL21. We speculate that the autoinhibitory intramolecular contacts between the C-terminal tail and chemokine body are disrupted by GAG binding and/or interactions with the CCR7 receptor to ensure optimal functionality.

Graphical Abstract

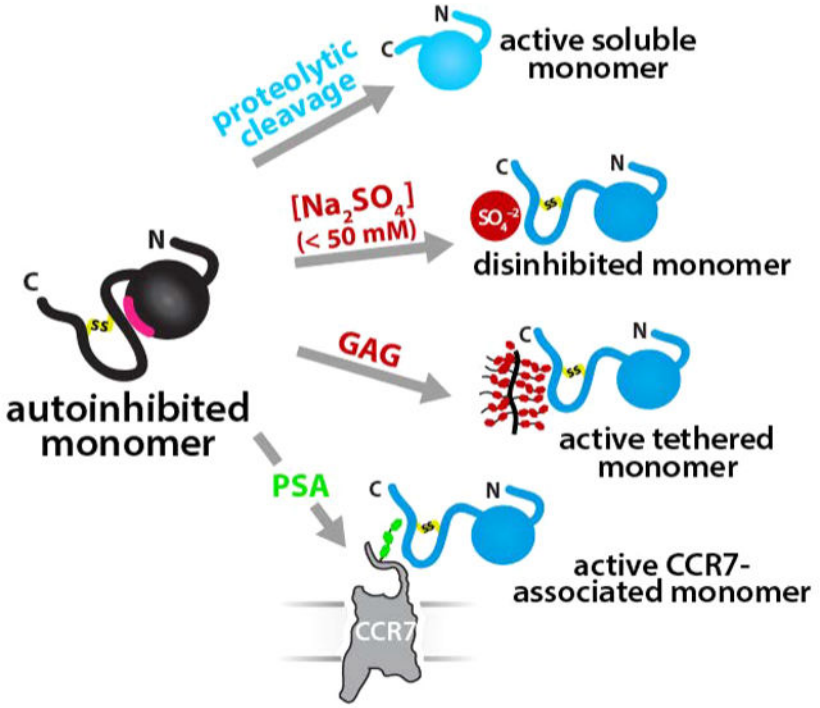

Chemokines are a family of small, 7–15 kDa, globular proteins that direct the migration of cells along an increasing chemokine concentration gradient (reviewed in refs 1 and 2). Chemotactic migration is accomplished via binding of the chemokine ligands to their receptors. Chemokine receptors are class A G-protein-coupled receptors that are prototypically linked to $G\alpha_i$ proteins that stimulate the mobilization of calcium from intracellular stores,[3,4] inhibition of adenylyl cyclase and thus cyclic adenosine monophosphate (cAMP),[5] and ultimately actin cytoskeletal rearrangement required for chemotaxis.[6,7] The chemokine family has a conserved structure that reflects the highly conserved cysteine residues and is subdivided into CC, CXC, CX3C, and XC based upon the

spacing of the conserved N-terminal cysteine residues.[8] The chemokines CCL21 and CCL19 are members of the CC chemokine family that bind the cognate receptor CCR7 to direct the migration of mature dendritic cells and naïve T cells to secondary lymphoid organs.[9,10] Both CCR7 ligands are transcytosed to high endothelial venules and expressed by stromal cells of secondary lymphoid organs, while CCL21 is also expressed in peripheral lymphatic vessels.[11–15] CCL21 is additionally able to bind GAGs and become immobilized via a 32 residue extended C-terminal tail,[16,17] not present in CCL19.[18,19] The paradigm that CCL19 and CCL21 act as redundant signaling molecules was challenged in 2009 with a report from the Lefkowitz laboratory, which indicated that CCL19 and CCL21 binding CCR7 resulted in distinct patterns of G-protein-coupled receptor kinase modification.[20] In this early example of GPCR "ligand bias", which has also been shown for other chemokines,[21,22] CCL19 and CCL21 were understood to activate different subsets of the full array of intracellular CCR7 effectors. However, the mechanisms by which CCL19 and CCL21 act as biased agonists for CCR7 remain poorly understood. Moreover, CCL19 and CCL21 are ligands for the atypical receptor ACKR4, a scavenger receptor regulating chemokine availabilities for CCR7,[23] further complicating the potential functions of these ligands.

Plasmin and dendritic cell-secreted proteases cleave the C-terminus of full-length CCL21 (CCL21WT, 111 residues, 12 kDa), producing an approximately 8 kDa chemokine variant that lacks affinity for GAGs.[24,25] However, the C-terminally truncated CCL21 protein remains functional, amplifying the ligand options for CCR7 activation.[24,26–29] CCL21WT and a C-terminally truncated variant, approximating the dendritic cell-digested CCL21 (CCL21trunc, residues 1–79, 8.8 kDa), have been shown in multiple studies to elicit different responses in functional assays including chemotaxis, calcium flux, cyclic AMP, β-arrestin recruitment, and receptor internalization.[26–28,30] NMR comparisons of CCL21WT and CCL21trunc revealed weak autoinhibitory interactions between the C-terminus and the folded chemokine domain.[28] Studies examining the effects of transferring the C-terminus of CCL21 to CCL19 have shown increases in heparin binding,[31] decreased chemotactic efficiency,[28] or no effect in chemotaxis, calcium flux, or CCR7 endocytosis.[27] These discrepancies between published studies suggest that each of the CCR7 ligands, CCL19, CCL21, and CCL21trunc, has a distinct signaling profile that may further be impacted by cell type, GAG diversity, and solution conditions, as observed for other chemokines.[32–36]

In addition to CCL21, XCL1, CXCL9, CXCL12γ, CCL16, CCL25, and CCL28 chemokines also possess a flexible C-terminal extension. However, these C-terminal domains retain little conserved sequence identity and do not appear to possess consensus functional roles among the various chemokines. Roles for the C-terminal tail in GAG-binding have been documented for CCL21, CXCL12γ, and CXCL9,[31,37–43] while the C-terminus of CCL28 and CXCL9 contributes to their antimicrobial activity.[33,44] The presence of a third disulfide bond is also unusual in the chemokine family, present in CCL21, CCL1, CCL15, CCL23, and CCL28. Only in CCL21 is the extra disulfide bond contained within the flexible C-terminal domain, providing a constraint to the otherwise disordered tail region.[16] The presence of the extended C-terminal tail has been shown to change the conformation of the chemokine core structure, as seen in comparisons of the 2D NMR HSQC spectra and the solved structures of CCL21WT and CCL21trunc.[28,45] However, the mechanism by which

the C-terminal tail alters CCL21 structure and influences chemokine function remains little understood.

Using biophysical and cell-based approaches, we identified distinct regions of the C-terminus that mediate structural and functional effects. Specifically, we showed that the chemokine-proximal region of the tail is essential for the previously identified autoinhibitory chemokine-tail interactions, while the distal region of the tail is responsible for functional differences seen between CCL21WT and CCL21trunc.

MATERIALS AND METHODS

Reagents.

Dulbecco's modified Eagle medium (DMEM), Roswell Park Memorial Institute (RPMI) 1640 ATCC formulation, Hanks' Balanced Salt Solution (HBSS) with calcium and magnesium, Dulbecco's PBS, Penicillin/Streptomycin (10,000 U/mL), 1 M HEPES, 100× minimum essential medium (MEM) non-essential amino acids solution, 100× GlutaMAX supplement, 100 mM sodium pyruvate, Geneticin (50 mg/mL), BSA Fraction V 7.5% v/v solution, TrypLE, fibronectin, and versene were purchased from Thermo Fisher Scientific (Waltham, MA, USA). Fetal bovine serum (FBS) was purchased from Atlanta Biological (Flowery Branch, GA). Calcium 6 dye was purchased from Molecular Devices (San Jose, CA, USA).

For the CHO and dendritic cell (DC) experiments, X-vivo 15 medium was from Lonza (Basel, Switzerland). $CaCl_2$, $MgCl_2$, glucose, HEPES, 2% v/v human Ab serum, 7.5% w/v Na_2HCO_3, MEM (10×), FBS, Penicillin/Streptomycin, glutamine, prostaglandin E_2 (PGE_2), forskolin, formaldehyde, and fluoromount were from Sigma (St. Louis, MO, USA). Human IL-4, GM-CSF, TNFα, IL-1β, and IL-6 were from Peprotech (Rocky Hill, NJ, USA). Lymphoprep was from STEMCELL technologies (Vancouver, Canada). The PureCol bovine collagen I suspension was from Advanced Biomatrix (Carlsbad, CA, USA).

Cell Culture.

All cells were incubated at 37 °C and 5% CO_2. CHEM-1 CCR7 cells (Eurofins, Luxembourg) were cultured in DMEM supplemented with 1% v/v Penicillin/Streptomycin, 10% v/v heat-inactivated FBS, 10 mM HEPES buffer, and 1× MEM nonessential amino acids. B16/F1 melanoma cells stably expressing CCR7 were graciously provided by Dr. Samuel T. Hwang (UC Davis) and cultured in DMEM supplemented with 1% v/v Penicillin/Streptomycin, 10% v/v FBS, 1× MEM nonessential amino acids, 1× GlutaMax, and 1 mM sodium pyruvate. Stable CCR7 expression was selected by culturing cells in full growth medium supplemented with 500 μg/mL Geneticin. Adherent cells were dislodged with TrypLE at approximately 90% confluence and passaged into new flasks. Stable cell lines were not used beyond passage 40. Human DCs were grown in X-vivo 15 medium with 2% v/v human AB serum and glutamine. CHO-K1 cells were grown in RPMI with 10% v/v FBS and Penicillin/Streptomycin. These cells were split routinely by dislodging in trypsin. HEK293T cells were cultured in DMEM supplemented with 1% v/v Penicillin/

Streptomycin, 10% v/v FBS, and 1× MEM nonessential amino acids. These cells were split routinely by dislodging in Versene.

DC Preparation.

DCs were prepared from human PBMCs isolated from buffy coats obtained from healthy donors by centrifugation on a Lymphoprep gradient. Briefly, monocytes were isolated by plastic adherence of PBMC. Adhered monocytes were subsequently cultured and differentiated into immature DCs by incubation with IL-4 (250 U/mL) and GM-CSF (1000 U/mL) for 6 days, followed by activation into mature DCs by incubation with IL-6 (1000 U/mL), IL-1β (1000 U/mL), TNFα (1000 U/mL), and PGE_2 (1 μg/mL) for an additional 2 days in the same medium. Stimulation medium was aspirated, and the remaining adherent DCs detached using ice-cold 5 mM EDTA in PBS. The cells lifted with a cell scraper, and aliquots of DCs were frozen and stored in liquid nitrogen.

Calcium Mobilization.

CHEM-1 CCR7 cells were grown in 96-well plates overnight to 80–90% confluency in DMEM with 1% v/v Penicillin/Streptomycin, 10 mM HEPES buffer, and 1× MEM nonessential amino acids. Media was removed, and 100 μL of assay buffer (1× HBSS, 20 mM HEPES, 0.1% v/v BSA Fraction V 7.5% solution) and 100 μL of Calcium 6 dye (prepared according to manufacturer's instructions) were added to each well. Cells were then incubated at 37 °C for 45 min. Chemokines were diluted in 1× HBSS, 20 mM HEPES, to 9× desired concentrations and plated in clear v-bottom wells. A Molecular Devices FlexStation3 was used to measure calcium flux upon the addition of 25 μL of chemokine. Fluorescence was measured every 1.52 s over 100 s in total. Minimum fluorescence measurements were subtracted from maximum fluorescence measurements for each well for the indicated biological replicates performed in triplicate. Mean and standard deviations were calculated and graphed using GraphPad Prism 7 (San Diego, CA, USA).

Bioluminescence Resonance Energy Transfer (BRET) cAMP Assay.

cAMP inhibition studies were performed as previously described.[27] Briefly, CHO cells were transiently transfected with human CCR7 and Camyel, which senses cAMP levels.[46] The following day, cells were loaded with the Camyel bioluminescent substrate coelenterazine and stimulated with chemokine, followed by forskolin that directly activates adenylate cyclase and increases intracellular cAMP levels. Forskolin was used to create a baseline production of cAMP for the $G\alpha_i$ subunit to inhibit upon activation of CCR7 through its ligands. The emission signal from enhanced yellow fluorescent protein (eYFP) and Renilla luciferase (Rluc) was measured using the envision machine at 530 and 480 nm and the BRET signal determined as the ratio between eYFP and Rluc. High cAMP correlates with the low BRET signal (Camyel in a conformation where eYFP and RLuc are far apart); thus, cAMP inhibition correlates positively with the BRET signal.

IncuCyte Chemotaxis.

Chemotaxis plates were first coated in 5 μg/mL fibronectin in 0.1% w/v BSA in Dulbecco's PBS. Then, 150 μL of the fibronectin solution was added to a reservoir plate (Essen

BioScience, Ann Arbor, MI), the chemotaxis insert was placed in the reservoir, and an additional 20 μL of fibronectin added the inset wells. After incubation for 1 h at room temperature, the fibronectin was aspirated from the reservoir and replaced with 200 μL of Dulbecco's-PBS. An additional 40 μL of Dulbecco's-PBS was added to each insert well, to be aspirated immediately before cell seeding.

B16 mouse melanoma cells stably expressing CCR7 were seeded onto the chemotaxis insert of desired wells at 1000 cells per well in 60 μL of 0.5% v/v FBS in the medium. Chemokine solutions were prepared in 0.5% v/v FBS media, and 200 μL of the mixture was added to triplicate reservoirs. The chemotaxis plate was then placed in the IncuCyte live-cell imaging platform at 37 °C, 5% CO_2 (Essen BioScience, Ann Arbor, MI), and imaged every hour using phase contrast and a 10× objective. Migration was calculated by determining the area on the bottom of the inset that was covered with cells using the IncuCyte analysis software.

Three-Dimensional (3D) Chemotaxis.

Chemotaxis assays were conducted as previously described.[26] Briefly, 45 μL of mature human monocyte-derived DCs suspended in X-vivo 15 medium with serum and glutamine (2×10^6 cells/mL) were added to a mixture of bovine collagen I (3%, 75 μL), Na_2HCO_3 (7.5%, 5 μL), and MEM (10×, 10 μL), and 6 μL of the final solution was loaded inside the Ibidi channel. After polymerization for 45 min, the Ibidi source and sink reservoirs were filled with chemokine containing medium and pure medium, respectively, as described in the manufacturer's instructions. Migration was tracked in a time-lapse microscope for 12 h at 2 min intervals. Cell migration (approximately 20–40 cells per viewing field) was tracked using a commercial tracking program (Autozell) and subsequently analyzed to get a population-based chemotactic index (CI) value (MATLAB). CI is a measure of net translocation distance to the source relative to the total distance traveled. Tracking was measured for a total distance of 1000 μm. Optimization experiments confirmed that most DCs leave the tracked field within 2–4 h, while new cells enter the field from the sink side.

Arrestin Recruitment Assays.

β-Arrestin 1 recruitment to CCR7 and ACKR4 induced by native and truncated chemokines was monitored by the NanoLuc complementation assay (NanoBiT, Promega), as previously described.[47–49] In brief, 5×10^6 HEK293T cells were seeded in 10 cm culture dishes and, 24 h later, cotransfected with pNBe vectors encoding CCR7 or ACKR4 C-terminally fused to SmBiT and human β-arrestin-1 N-terminally fused to LgBiT. Cells were harvested 24 h post-transfection, incubated 25 min at 37 °C with the 200-fold diluted Nano-Glo live-cell substrate, and distributed into white-walled 96-well plates (5×10^4 cells per well). Upon the addition of chemokines at concentrations ranging from 30 pM to 1 μM, β-arrestin recruitment to CCR7 and ACKR4 was evaluated with a Mithras LB940 luminometer (Berthold Technologies).

Preparation of CCL21WT (1–111).

Human CCL21 was expressed in *Escherichia coli* as a fusion protein containing hexa-histidine-tagged SMT3 (SUMO) on a pQE30 plasmid (kindly provided by Dr. Christopher Veldkamp, University of Wisconsin, Whitewater). BL21 (pREP4) competent *E. coli* were

transformed with the pQE-His6-SMT3-CCL21 plasmid. Transformants were grown in 1 L of Terrific Broth or U–^{15}N M9 minimal media supplemented with 150 μg/mL ampicillin and 50 μg/mL kanamycin at 37 °C to an optical density at 600 nm of 1.0. They were induced with 1 mM isopropyl β-D-1-thiogalactopyranoside and harvested the following day or allowed to grow at 37 °C in U–^{15}N M9 media or 5 h at 37 °C followed by 4 °C overnight in Terrific Broth. Cell pellets were lysed via French press and centrifuged at 15,000*g* for 30 min. The resolubilized inclusion body pellet was clarified by centrifugation and loaded onto a Ni-IDA (Clontech) column. The fusion protein was eluted with 100 mM sodium acetate pH 4.5, 6 M guanidine HCl, 300 mM sodium chloride, 10 mM imidazole, and dialyzed against 0.3% v/v acetic acid at 4 °C. The fusion protein was refolded in 20 mM Tris pH 8.0 via dialysis and cut with ULP-1 (ubiquitin-like-specific protease 1) to provide a native N-terminus. CCL21 protein was separated from its His-SUMO tag via cation exchange chromatography (SP Sepharose Fast Flow resin, GE Healthcare UK Ltd.) and further purified by a reverse-phase HPLC column, eluted with a gradient of acetonitrile in 0.1% v/v trifluoroacetic acid. Proteins were lyophilized and analyzed for purity and proper folding using mass spectrometry and NMR spectroscopy.

CCL21 C-terminus mutant plasmids were created by the addition of stop codons for the truncations, and cysteine to alanine mutation for the cysteine mutants using site-directed mutagenesis (Agilent, Santa Clara, CA). The following CCL21 mutants were made using a pQE-His6-SMT3 vector: CCL21 T102stop; CCL21 C80A K92stop; CCL21 C80AC99A; CCL21 1–91 C80A, CCL21 1–79, CCL21 C80AC99A, and CCL21 1–79 proteins were prepared as described previously.[50]

Nuclear Magnetic Resonance Spectroscopy.

NMR spectroscopic data were collected at the NMR facility at the Medical College of Wisconsin on a Bruker Avance 600 MHz spectrometer equipped with a 1H/^{13}C/^{15}N cryoprobe. 15N-Labeled chemokine (various CCL21 mutants) were diluted in 25 mM deuterated MES pH 6.0 with 10% v/v D_2O and 0.02% v/v NaN_3. ^{15}N–^{1}H heteronuclear single quantum coherence (HSQC) spectra were collected for each chemokine variant. NMR samples that were directly compared in HSQC overlays were buffer matched to the control for variations in buffer preparation.

Chemical shift perturbations (CSPs) between the peaks of each CCL21 mutant were quantified as previously described.[51] Briefly, total 15N–^{1}H chemical shift perturbations were computed as $[(5\Delta\delta_{NH})^2 + (\Delta\delta_N)^2]^{1/2}$, where $\Delta\delta_{NH}$ and $\Delta\delta_N$ were the total changes in backbone amide 1H and 15N chemical shifts in ppm, respectively, between the CCL21 variant spectra. Shifting peaks were assigned from the NMR solution structure assignments of CCL21WT (CARA template files graciously provided by Dr. Christopher Veldkamp), and the nearest signal attributed when peak locations were perturbed.

Monomer–dimer equilibrium fit calculations were performed with pro Fit 6.2.16 (QuantumSoft, Switzerland) and the following equation adapted from ref 32 for CSP instead of the fluorescence polarization signal:

$$\Delta\delta = (\Delta\delta_{\text{dimer}} - \Delta\delta_{\text{monomer}}) \times \frac{\left(\left(K_d^2 + 8xK_d\right)^{0.5} - K_d\right)^2}{8xK_d} + \Delta\delta_{\text{monomer}}$$

where $\Delta\delta$ is the CSP, K_d is the CCL21 dimer dissociation constant, and x is the CCL21 concentration.

^{1}H, ^{15}N Heteronuclear NOE Experiments.

^{15}N heteronuclear NOEs were measured using the Bruker hsqcnoef3gpsi pulse program. The heteronuclear NOE values were calculated as a ratio of peak intensities from spectra collected with and without proton saturation.

RESULTS

The Flexible CCL21 C-Terminus Participates in Concentration-Dependent Conformational Changes.

To confirm that the flexible CCL21 C-terminus interacts with the folded chemokine domain,[28] we compared 2D ^{15}N–^{1}H HSQC spectra of CCL21WT with a previously described CCL21 truncation variant, CCL21 trunc,[26,27,31,37,38,45,52] employed as a surrogate for the DC protease-cleaved molecule (Figure 1a). Truncation-induced chemical shift differences (Figure 1b), similar to those described by Kiermaier et al.,[28] clustered at the C-terminal end of the α-helix. Upon comparison of the NMR solution structure of CCL21WT (PDB ID: 2L4N) and the crystal structure of CCL21trunc (PDB ID: 5EKI), we observed that truncation-induced chemical shift perturbations coincided with a section of the helix that is bent in CCL21WT and straight in CCL21trunc (Figure 1c).

We next compared the 15N–^{1}H heteronuclear NOE (hetNOE) values at 600 MHz for CCL21WT (Figure 1d) and CCL21trunc (Figure 1e) as a measure of backbone flexibility on picosecond–nanosecond time scales. These NMR analyses of CCL21WT and CCL21trunc demonstrated that the C80–C99 disulfide bond increased local stability in the otherwise unstructured tail, as illustrated by the positive NOE values centered at residues 80 and 99. Our data in Figure1d agree with a prior NMR structural analysis of full-length CCL21WT.[16] The hetNOE profiles for equivalent regions of CCL21WT and CCL21trunc were largely comparable, with both exhibiting dynamic N-termini and structured core domains.

Many chemokines form homodimers or exhibit conformational variability in different solution conditions. For example, dimerization of CXCL12 is enhanced by the addition of phosphate or sulfate,[32] while XCL1 dimerization is diminished with the addition of sodium chloride,[53] and the helix of CXCL12 undergoes a conformational change in the transition from monomer to the dimer.[54] While a previous analytical ultracentrifugation analysis of CCL21 self-association detected no dimerization at concentrations as high as 200 μM,[16] we noticed that peak positions varied for several residues in the HSQC spectra of CCL21 recorded at different concentrations in the 20 μM to 2 mM range. Thus, before investigating the role of the C-terminal domain on CCL21 structure and function in greater detail, we surveyed the effect of solution conditions on the CCL21 structure using 2D NMR. In 2D

^{15}N–^{1}H HSQC spectra for CCL21WT at concentrations ranging from 20 μM to 2 mM, a subset of CCL21 residues (C9, L10, V21, V22, R23, E29, S31, K75) shifted along a linear trajectory consistent with a two-state equilibrium process in fast exchange (Figure 2a, full spectra in Figure S1). Estimates of the dimer K_d from the nonlinear fitting of concentration-dependent shifts varied from 2–10 mM for different residues, indicating that CCL21 self-association is a weak interaction that would likely be imperceptible by most analytical methods including analytical ultracentrifugation. Interestingly, a set of residues at the end of the helix (M64, H66, L67, D68, K69, T70, and Q78) shifted in two different directions in spectra acquired at CCL21WT concentrations above and below 800 μM. The total displacements were typically larger than the other peaks that shifted unidirectionally (Figure 2b) and comparable to truncation-induced shifts shown in Figure 1b. A similar HSQC titration of CCL21trunc showed only unidirec tional peak movement (Figure 2c, full spectra in Figure S2) and smaller concentration-dependent shifts than CCL21WT (Figure 2d). Residues of CCL21trunc near the N-terminus (which participates in CC-type dimer interfaces) as well as the β1 strand (which mediates CXC-type dimerization) exhibited concentration-dependent shifts but did not cluster in a manner that could be reliably ascribed to canonical CC or CXC chemokine dimerization. Bidirectional peak shifts observed in the CCL21WT dilution series suggest the C-terminus may participate in a multistate equilibrium that involves dimerization and conformational change.

CCL21 Structure Differences Minimized with Increasing Salt Concentrations.

To evaluate the effect of solution conditions on CCL21 self-association, we recorded the HSQC spectra of 200 μM CCL21WT in increasing concentrations of sodium sulfate or sodium chloride. Notably, sodium sulfate induced chemical shift changes in the spectra (Figure 2e) that were markedly opposite to the effect observed in the CCL21 dilution experiments. Thus, a subset of CCL21WT peaks (e.g., K69 and T70) that had bidirectional chemical shift perturbations (CSP) in the dilution series (Figure 2a) exhibited bidirectional shifts in response to increasing concentrations of Na_2SO_4 (Figure 2e). As the shifts observed upon the first addition of Na_2SO_4 (20 mM) were reminiscent of the shifts induced by C-terminal truncation (Figure 2f), we compared the spectra of CCL21WT and CCL21trunc in the presence of 20 mM Na_2SO_4 (Figure 2g). These HSQC spectra were nearly superimposable, suggesting that the addition of Na_2SO_4 disrupts the effect of the flexible CCL21 C-terminus on the chemokine domain.

A similar comparison of titrations with NaCl showed simple unidirectional peak shifts for both CCL21WT and CCL21trunc (Figure 2h). Strikingly, the peaks for all residues that exhibited truncation-dependent shifts (Figure 2f) again shifted toward a single position, suggesting that an increase in solution ionic strength diminished the effect of the C-terminal tail. Moreover, the pattern of NaCl-induced shifts was the reverse of CCL21 concentration-dependent shifts (Figure 2a,b), suggesting that dimerization is favored by an increase in solution ionic strength.

On the basis of the NMR comparisons of CCL21WT and CCL21trunc at different concentrations and solution conditions, we concluded that CCL21 has a weak propensity to self-associate and that increased solution ionic strength stabilizes the dimer. We speculate

that the flexible C-terminal tail forms specific, weak contacts with the chemokine domain and that these interactions occur only when the chemokine is monomeric. Since CCL21 self-association is minimal at the conditions used for our initial structural comparisons of CCL21WT and CCL21trunc, we propose that the truncation-induced shifts in Figure 1a and Figure 1b arise predominantly from the loss of interactions between some portion of the flexible C-terminal tail comprised of residues 80–111 and the folded chemokine domain.

CCL21WT and CCL21trunc Have Different Functional Profiles.

Having demonstrated the structural impact of the C-terminus on CCL21 conformation, we examined its ability to modulate CCL21 activation of CCR7 and the atypical chemokine receptor ACKR4. As shown in Figure 3a, both CCL21WT and CCL21trunc induced robust calcium mobilization, a measure of G-protein activation, in CCR7-expressing CHEM1 cells. CCL21trunc was a more potent agonist (EC_{50} = 6 nM for CCL21trunc versus 33 nM for CCL21WT). Similar potency differences were also observed in CCR7-expressing B16 melanoma cells (Figure S3a). We next tested inhibition of cyclic adenosine monophosphate (cAMP) downstream of $G\alpha_i$ as a second readout for G-protein activation following ligand binding to CCR7. As shown in Figure 3b, we observed a 20-fold difference in activity, with CCL21trunc again more potent than CCL21WT (EC_{50} = 1.5 nM for CCL21trunc versus 20.2 nM for CCL21WT). Consistent with previous reports, stimulation of ACKR4-expressing cells with CCL21WT induced no G-protein signaling (data not shown). Using a Nanoluciferase complementation-based assay to measure chemokine-induced recruitment of β-arrestin 1 to the receptor C-terminus, we found that CCL21trunc was approximately twice as potent as CCL21WT acting on CCR7 (EC_{50} values of 60 and 120 nM, respectively) and 3-fold more potent for ACKR4 (EC_{50} values of 7 and 22 nM, respectively) (Figure 3c). Next, we examined the functional consequences of CCL21-induced signaling with a live-cell imaging platform measuring 2D transwell chemotaxis. In agreement with calcium mobilization and cAMP synthesis inhibition, we observed that CCL21trunc was more potent, stimulating migration at lower concentrations than CCL21WT. However, CCL21WT was more efficacious in an extended dose–response curve performed in B16 melanoma cells (Figure 3d). This pattern of potency versus efficacy was similar to those observed by Hauser et al.,[30] who used a truncated variant of CCL21, containing residues 1–75. We also tested these chemokines in a 3D chemotaxis platform using human dendritic cells and observed CCL21trunc was more efficacious than CCL21WT at 10 nM (Figure S3b) agreeing with a prior report.[26] Taken together, the results demonstrate that the CCL21 C-terminus alters its CCR7 activation profile. To identify specific regions within the C-terminus that are responsible for the structural and functional differences between CCL21WT and CCL21trunc, we constructed a panel of CCL21 variants shown in Figure 3e.

C-Terminal Truncation Reveals Two Important Regions for CCL21 Activity.

We next probed the C80–C99 disulfide bond, which creates a cyclic 20 residue peptide within an otherwise flexible, 42 residue C-terminal tail distal to the end of the α-helix. Chemical shift perturbations in the CCL21 C80AC99A HSQC spectrum relative to CCL21WT were localized to residues 79–97 (Figure 4a,b), consistent with loss of the C80–C99 disulfide. The negative ^{15}N–^{1}H hetNOE values for these residues (Figure S4) were lower than we showed in Figure 1d for CCL21WT due to the absence of the disulfide. In

calcium flux, cAMP, and chemotaxis assays, the CCL21 C80AC99A disulfide mutant was not significantly different from CCL21WT, except at a single 3 μM concentration for chemotaxis in which it had approximately 40% lower efficacy (Figure 4c–e). No difference in potency or efficacy of β-arrestin 1 recruitment to either CCR7 or ACKR4 was observed between CCL21WT and CCL21 C80AC99A (data not shown). Thus, the elimination of the C80–C99 disulfide had no significant impact on CCL21 structure or function.

Comparisons of the HSQC spectra of two truncation mutants (CCL21 1–101 and CCL21 1–91 C80A) with those of CCL21WT and CCL21trunc showed that removal of residues 92–111 induced a few small changes in peak position, while the majority of the observed shifts occurred only upon removal of residues 80–90 (Figure 5a). To quantify these changes, we plotted the CSP between the CCL21 1–91 C80A and CCL21trunc spectra (Figure 5b, full spectra in Figure S5a). The CSP plot was remarkably similar to the plot comparing CCL21WT and CCL21trunc spectra (Figure 1b). Thus, each of the longer truncation variant spectra overlaid nearly identically, with only the CCL21trunc spectrum demonstrating marked chemical shift perturbations (Figure 5a). This pattern was even more apparent at 200 μM (Figure S5b). The hetNOE profiles for these truncation variants followed the previous pattern established by CCL21WT, CCL21trunc, and CCL21 C80AC99A (Figure S5c). The hetNOE of CCL21 1–101 confirmed that the disulfide bond within the C-terminus of CCL21 1–101 conferred stability in an otherwise dynamic loop region, as demonstrated with the positive NOE values in the C-terminus surrounded by residues with negative NOE values. The CCL21 1–91 C80A variant, which lacks the disulfide, had a highly dynamic C-terminus, as evidenced by the increasingly negative hetNOE values (Figure S5c). Cumulatively, these structural analyses of the truncation mutants suggest that one or more amino acids in the region from residues 80 to 91 are responsible for chemical shift perturbations changes observed in the folded chemokine domain upon removal of the CCL21 C-terminal domain.

When we subjected these truncation variants to the functional assays, a consistent divergence from the structural analyses emerged. In these assays, CCL21trunc and CCL21 1–91 C80A performed comparably and were different from the CCL21 1–101 variant lacking only 10 residues and CCL21WT (Figure 5c–e). As shown in Figure 5c, CCL21 1–91 C80A was more potent than the longer CCL21 1–101 variant in mobilizing intracellular calcium with an EC_{50} = 7 nM versus 21 nM, respectively. In cAMP inhibition assays, the CCL21 1–91 C80A mutant protein activated $G\alpha_i$ in a similar fashion as the CCL21trunc variant, exhibiting a sigmoidal dose–response curve from 10 pM to 100 nM (EC_{50} = 7 nM). In contrast, CCL21 1–101 and CCL21WT were unable to activate the $G\alpha_i$ protein to decrease cAMP production (Figure 5d). While differences in EC_{50} obtained from nonlinear fitting failed to reach statistical significance ($p > 0.05$, one-way ANOVA), measurements of β-arrestin 1 recruitment to CCR7 and ACKR4 (Figure 5e) suggested that CCL21WT and CCL21 1–101 were slightly more potent (CCR7 EC_{50} ~ 100 nM; ACKR4 EC_{50} ~ 30 nM), than CCL21 1–91 C80A and CCL21trunc (CCR7 EC_{50} ~ 60 nM; ACKR4 EC_{50} ~ 5 nM). Taken together, these results demonstrate that the shorter CCL21 variants, CCL21trunc and CCL21 1–91 C80A, are more potent agonists for CCR7 compared to longer and full-length chemokines and that a similar trend may hold for the atypical receptor ACKR4.

Interestingly, chemotaxis, a functional outcome downstream of receptor activation, of CCR7-expressing B16 melanoma cells indicated that the shorter chemokines, CCL21trunc and CCL21 1–91 C80A, retained elevated potency, but were less efficacious in a full dose–response curve than the longer chemokines, CCL21 1–101 and CCL21WT (Figure 5f). The increased potency was not restricted to a single cell line, as we also observed the same relative relationship, with the shorter CCL21 variants being more potent, in primary human DCs (Figure S5d). Taken together, these data from the calcium mobilization, cAMP inhibition, and chemotaxis assays suggest residues 92–100 are responsible for the functional differences between CCL21WT and CCL21trunc. In contrast, NMR chemical shift comparisons implicated residues 80–90 as the region of the flexible C-terminal domain that induces most of the structural differences between CCL21WT and CCL21trunc.

DISCUSSION

Functional selectivity, also known as biased agonism, is an emerging pharmacological signaling mechanism wherein distinct ligands can bind to the same G-protein-coupled receptor and activate a subset of that receptors total signaling repertoire.[55] We have previously shown that structural changes in a chemokine ligand orchestrate their function as biased agonists.[56–59] As a protein family, chemokines adopt a distinctive structure consisting of a three-stranded β-sheet and C-terminal helix stabilized by a pair of conserved disulfide bonds.[16,18,60] While CCL19 and CCL21 both activate the CCR7 receptor, they share only 31% sequence identity within the chemokine domain, and CCL19 lacks the CCL21 flexible 32 amino acid C-terminal tail, which also contains an unusual third disulfide bond.[17] Several reports have previously shown distinct profiles of biased signaling for the CCR7 ligands CCL21 and CCL19 that are not due to differences in their N-terminal sequences,[20,26,61,62] and others have observed functional differences between full-length and C-terminally truncated CCL21.[26–28,30] Having previously shown roles for polysialylation of CCR7 in relieving CCL21 autoinhibition, we used NMR to probe potential roles for the C-terminal tail in signaling.

As shown here and observed previously by Jorgensen et al.,[27] deletion or removal of the tail by a DC-specific protease[24,25] enhances its CCR7 agonist activity as measured by cAMP inhibition. We were perplexed by the near-absence of cAMP inhibition by 100 nM CCL21WT when the Ca^{2+}-flux response is maximal at the same concentration since chemokine receptors are thought to primarily activate the $G\alpha_{i/o}$ family of heterotrimeric G-proteins. However, the PRECOG (*Pre*dicting *co*upling probabilities of *G*-protein-coupled receptors) algorithm, developed by the Russell lab from their recent analysis of coupling between 148 GPCRs and 11 different $G\alpha$ C-termini,[63] predicts that CCR7 will couple to only one of the four $G_{i/o}$ proteins with a probability of 0.7 and is more likely to couple to the G12/13, $G_{q/11}$, and G_s families (PRECOG probabilities of 0.8, 0.9, and 0.9, respectively). The apparent discrepancy in cAMP and Ca^{2+} responses to CCL21WT may, therefore, be due to CCR7 coupling to non-Gi family members. Future studies will investigate the ability of CCR7 to couple to different $G\alpha$ families and the effect of CCL21 truncation on the $G\alpha$ coupling profile.

Owing to an abundance of basic amino acids (Arg or Lys at 12 of 32 positions), the tail confers high-affinity GAG binding to CCL21,[31,38] needed for accumulation within lymphatic vessels.[64] Transfer of the CCL21 tail to CCL19 enhances its GAG binding[31] and reduces its potency in cAMP inhibition assays.[27] Moreover, reports from two different groups indicated that CCL19 and CCL21 act as biased agonists, activating downstream CCR7 signaling pathways to different extents.[20,26,30,61] Other studies ascribe higher chemotactic efficacy to CCL21WT (more cells migrated) but greater potency to CCL21trunc.[26,28,29] Finally, comparisons of the structures solved by NMR spectroscopy and X-ray crystallography suggest that CCL21WT and CCL21trunc adopt different conformations.[16,45] Of note, the profile of truncation-induced chemical shift perturbations in CCL21 was very similar to the shift perturbation profiles of binding to heparin,[31] polysialic acid (PSA),[28] or a short sulfopeptide from the CCR7 N-terminus.[65] While no systematic analysis of individual residues or segments has been performed, an abundance of previous studies established that the C-terminal tail likely makes autoinhibitory contacts with and modulates the structure and function of the CCL21 chemokine domain.[28]

We postulated that specific regions of the C-terminus were responsible for the structural and functional dynamism of CCL21. To test this hypothesis, we created a series of CCL21 C-terminal truncation mutants as well as a variant lacking the third disulfide bond. Unexpectedly, we discovered that CCL21 self-association previously undetected by analytical ultracentrifugation was enhanced in solutions of high ionic strength and characterized by HSQC peak shifts that mirror those induced by truncation or binding to heparin,[31] PSA,[28] CCR7,[65] or sulfate ions. Our NMR results reveal that CCL21 conformational dynamics are likely influenced by many intraligand and extra-ligand interactions (Figure 6). Our data suggest that weak intramolecular interactions between the folded chemokine domain and the flexible C-terminus are disrupted by low concentrations of sulfate, reproducing the effects of truncation. Higher concentrations of sulfate or NaCl promote self-association of both CCL21WT and CCL21trunc, which converge on a common HSQC chemical shift profile. Since self-association had minimal effect on HSQC peak intensities and line widths and many chemokines are known to dimerize, we tentatively concluded that CCL21 exists in a very weak (K_d > 1 mM) monomer–dimer equilibrium. Because chemokines typically function at nanomolar concentrations where the monomeric species should dominate, and the crystal structure of CCL21trunc revealed no dimer interface,[45] the relevance of dimerization to CCL21 function seems remote. To minimize the confounding effects of oligomerization, we conducted our subsequent NMR measurements on CCL21 variants at 200–700 μM in low salt conditions.

The NMR results suggest that truncation-induced chemical shifts arise from weak interactions between the end of the α-helix and tail residues 80–90 and that those intramolecular contacts are present only when CCL21 is monomeric (Figure 6). Functional assays on the same panel of CCL21 variants implicated an adjoining region of the C-terminus (residues 92–100) in the lower potency (Ca^{2+}-flux and cAMP inhibition) and higher efficacy (chemotaxis) observed for full-length CCL21 relative to CCL21trunc. The profile of truncation-induced chemical shift perturbations in the CCL21 NMR spectra was reminiscent of the shifts induced by heparin,[31] PSA,[28] or a short sulfopeptide from the CCR7 N-terminus.[65] Our interpretation is that GAGs or the polysialylated and sulfotyrosine-

containing CCR7 N-terminus disrupt autoinhibitory interactions between the C-terminal tail and the helix, in much the same way that dimerization and sulfate binding mimic truncation of the C-terminal tail. Cumulatively, our data suggest that target cell chemotaxis is promoted by proteases, the receptor N-terminus, or GAGs, the combination of which facilitates the recruitment of DCs to peripheral lymphatic tissues.

In sum, we have probed the CCL21 C-terminus to identify autoinhibitory structural contacts. We showed via NMR spectroscopy that the region of the C-terminus between residues 80–90 is responsible for conformational changes that occur upon CCL21 truncation. We further showed that the region between residues 92–100 had the greatest effect on CCL21 potency and efficacy in calcium mobilization, cAMP synthesis inhibition, and chemotaxis assays. Factors such as locally increased CCL21 concentrations via binding to GAGs, binding to polysialic acid, or sulfated tyrosine on the CCR7 N-terminus, C-terminal truncation, or other as yet unknown interactions may disrupt intramolecular interactions and increase CCL21's functional potency as a CCR7 agonist and chemoattractant. We conclude that biased agonist variability of CCL21 functional responses within lymphatic vessels and secondary lymphoid organs reflects dynamic changes in chemokine structure that influence intracellular signaling by its receptor CCR7.

Supplementary Material

Refer to Web version on PubMed Central for supplementary material.

ACKNOWLEDGMENTS

We thank Dr. Christopher T. Veldkamp (University of Wisconsin, Whitewater) for providing the full-length CCL21 pdb file, CCL21 pQE30 plasmid, CCL21WT CARA template files, and helpful discussions.

Funding

This work is supported in part by grants from the National Institutes of Health including F30 CA210587 to N.A.M., AI058072 and GM097381 to B.F.V., and U01 CA178960 and R01 CA226279 to M.B.D. Additional support was also provided to M.B.D. by the Advancing a Healthier Wisconsin Endowment and continuing philanthropic support from the Bobbie Nick Voss Charitable Foundation. N.A.M. is a member of the Medical Scientist Training Program at MCW, which is partially supported by a training grant from NIGMS T32-GM080202.

ABBREVIATIONS

ACKR	atypical chemokine receptor
BRET	bioluminescence resonance energy transfer
cAMP	cyclic adenosine monophosphate
CCL	C–C motif chemokine ligand
CCR	C–C motif chemokine receptor
CSP	chemical shift perturbation
DC	dendritic cell

eYFP	enhanced yellow fluorescent protein
GAG	glycosaminoglycan
hetNOE	heteronuclear nuclear Overhauser effect
HSQC	heteronuclear single quantum coherence
K_d	equilibrium dissociation constant
Rluc	Renilla luciferase
SEM	standard error of the mean

REFERENCES

(1). Bachelerie F, Ben-Baruch A, Burkhardt AM, Combadiere C, Farber JM, Graham GJ, Horuk R, Sparre-Ulrich AH, Locati M, Luster AD, Mantovani A, Matsushima K, Murphy PM, Nibbs R, Nomiyama H, Power CA, Proudfoot AE, Rosenkilde MM, Rot A, Sozzani S, Thelen M, Yoshie O, and Zlotnik A (2014) International Union of Basic and Clinical Pharmacology. [corrected]. LXXXIX. Update on the extended family of chemokine receptors and introducing a new nomenclature for atypical chemokine receptors. Pharmacol. Rev 66, 1–79. [PubMed: 24218476]

(2). Thelen M, and Stein JV (2008) How chemokines invite leukocytes to dance. Nat. Immunol 9, 953–959. [PubMed: 18711432]

(3). Rossi DL, Vicari AP, Franz-Bacon K, McClanahan TK, and Zlotnik A (1997) Identification through bioinformatics of two new macrophage proinflammatory human chemokines: MIP-3alpha and MIP-3beta. J. Immunol 158, 1033–1036. [PubMed: 9013939]

(4). Agle KA, Vongsa RA, and Dwinell MB (2010) Calcium mobilization triggered by the chemokine CXCL12 regulates migration in wounded intestinal epithelial monolayers. J. Biol. Chem 285, 16066–16075. [PubMed: 20348095]

(5). Bokoch GM (1995) Chemoattractant signaling and leukocyte activation. Blood 86, 1649–1660. [PubMed: 7654998]

(6). Servant G, Weiner OD, Herzmark P, Balla T, Sedat JW, and Bourne HR (2000) Polarization of chemoattractant receptor signaling during neutrophil chemotaxis. Science 287, 1037–1040. [PubMed: 10669415]

(7). Chodniewicz D, and Zhelev DV (2003) Novel pathways of F-actin polymerization in the human neutrophil. Blood 102, 2251–2258. [PubMed: 12763941]

(8). Bacon K, Baggiolini M, Broxmeyer H, Horuk R, Lindley I, Mantovani A, Maysushima K, Murphy P, Nomiyama H, Oppenheim J, Rot A, Schall T, Tsang M, Thorpe R, Van Damme J, Wadhwa M, Yoshie O, Zlotnik A, Zoon K, and Nomenclature, I. W. S. o. C. (2002) Chemokine/chemokine receptor nomenclature. J. Interferon Cytokine Res 22, 1067–1068. [PubMed: 12433287]

(9). Willimann K, Legler DF, Loetscher M, Stuber Roos R, Belen Delgado M, Clark-Lewis I, Baggiolini M, and Moser B (1998) The chemokine SLC is expressed in T cell areas of lymph nodes and mucosal lymphoid tissues and attracts activated T cells via CCR7. Eur. J. Immunol 28, 2025–2034. [PubMed: 9645384]

(10). Saeki H, Moore AM, Brown MJ, and Hwang ST (1999) Cutting Edge: Secondary Lymphoid Tissue Chemokine (SLC) and CC Chemokine Receptor (CCR7) Participate in the Emigration Pathway of Mature Dendritic Cells from the Skin to Regional Lymph Nodes. J. Immunol 162, 2472–2475. [PubMed: 10072485]

(11). Ngo VN, Lucy Tang H, and Cyster JG (1998) Epstein-Barr Virus–induced Molecule 1 Ligand Chemokine Is Expressed by Dendritic Cells in Lymphoid Tissues and Strongly Attracts Naive T Cells and Activated B Cells. J. Exp. Med 188, 181–191. [PubMed: 9653094]

(12). Luther SA, Tang HL, Hyman PL, Farr AG, and Cyster JG (2000) Coexpression of the chemokines ELC and SLC by T zone stromal cells and deletion of the ELC gene in the plt/plt mouse. Proc. Natl. Acad. Sci. U. S. A 97, 12694–12699. [PubMed: 11070085]

(13). Gunn MD, Kyuwa S, Tam C, Kakiuchi T, Matsuzawa A, Williams LT, and Nakano H (1999) Mice lacking expression of secondary lymphoid organ chemokine have defects in lymphocyte homing and dendritic cell localization. J. Exp. Med 189, 451–460. [PubMed: 9927507]

(14). Carlsen HS, Haraldsen G, Brandtzaeg P, and Baekkevold ES (2005) Disparate lymphoid chemokine expression in mice and men: no evidence of CCL21 synthesis by human high endothelial venules. Blood 106, 444–446. [PubMed: 15863780]

(15). Baekkevold ES, Yamanaka T, Palframan RT, Carlsen HS, Reinholt FP, von Andrian UH, Brandtzaeg P, and Haraldsen G (2001) The Ccr7 Ligand ELC (Ccl19) Is Transcytosed in High Endothelial Venules and Mediates T Cell Recruitment. J. Exp. Med 193, 1105–1112. [PubMed: 11342595]

(16). Love M, Sandberg JL, Ziarek JJ, Gerarden KP, Rode RR, Jensen DR, McCaslin DR, Peterson FC, and Veldkamp CT (2012) Solution structure of CCL21 and identification of a putative CCR7 binding site. Biochemistry 51, 733–735. [PubMed: 22221265]

(17). Hromas R, Kim CH, Klemsz M, Krathwahl M, Fife K, Cooper S, Schnizlein-Bick C, and Broxmeyer HE (1997) Isolation and Characterization of Exodus-2, a Novel C-C Chemokine with a Unique 37-Amino Acid Carboxyl-Terminal Extension. J. Immunol 159, 2554–2558. [PubMed: 9300671]

(18). Veldkamp CT, Kiermaier E, Gabel-Eissens SJ, Gillitzer ML, Lippner DR, DiSilvio FA, Mueller CJ, Wantuch PL, Chaffee GR, Famiglietti MW, Zgoba DM, Bailey AA, Bah Y, Engebretson SJ, Graupner DR, Lackner ER, LaRosa VD, Medeiros T, Olson ML, Phillips AJ, Pyles H, Richard AM, Schoeller SJ, Touzeau B, Williams LG, Sixt M, and Peterson FC (2015) Solution Structure of CCL19 and Identification of Overlapping CCR7 and PSGL-1 Binding Sites. Biochemistry 54, 4163–4166. [PubMed: 26115234]

(19). Yoshida R, Imai T, Hieshima K, Kusuda J, Baba M, Kitaura M, Nishimura M, Kakizaki M, Nomiyama H, and Yoshie O (1997) Molecular cloning of a novel human CC chemokine EBI1-ligand chemokine that is a specific functional ligand for EBI1, CCR7. J. Biol. Chem 272, 13803–13809. [PubMed: 9153236]

(20). Zidar DA, Violin JD, Whalen EJ, and Lefkowitz RJ (2009) Selective engagement of G protein coupled receptor kinases (GRKs) encodes distinct functions of biased ligands. Proc. Natl. Acad. Sci. U. S. A 106, 9649–9654. [PubMed: 19497875]

(21). Steen A, Larsen O, Thiele S, and Rosenkilde MM (2014) Biased and g protein-independent signaling of chemokine receptors. Front. Immunol 5, 277. [PubMed: 25002861]

(22). Hauser MA, and Legler DF (2016) Common and biased signaling pathways of the chemokine receptor CCR7 elicited by its ligands CCL19 and CCL21 in leukocytes. J. Leukocyte Biol 99, 869–882. [PubMed: 26729814]

(23). Gosling J, Dairaghi DJ, Wang Y, Hanley M, Talbot D, Miao Z, and Schall TJ (2000) Cutting edge: identification of a novel chemokine receptor that binds dendritic cell- and T cell-active chemokines including ELC, SLC, and TECK. J. Immunol 164, 2851–2856. [PubMed: 10706668]

(24). Schumann K, Lammermann T, Bruckner M, Legler DF, Polleux J, Spatz JP, Schuler G, Forster R, Lutz MB, Sorokin L, and Sixt M (2010) Immobilized chemokine fields and soluble chemokine gradients cooperatively shape migration patterns of dendritic cells. Immunity 32, 703–713. [PubMed: 20471289]

(25). Lorenz N, Loef EJ, Kelch ID, Verdon DJ, Black MM, Middleditch MJ, Greenwood DR, Graham ES, Brooks AE, Dunbar PR, and Birch NP (2016) Plasmin and regulators of plasmin activity control the migratory capacity and adhesion of human T cells and dendritic cells by regulating cleavage of the chemokine CCL21. Immunol. Cell Biol 94, 955–963. [PubMed: 27301418]

(26). Hjorto GM, Larsen O, Steen A, Daugvilaite V, Berg C, Fares S, Hansen M, Ali S, and Rosenkilde MM (2016) Differential CCR7 Targeting in Dendritic Cells by Three Naturally Occurring CC-Chemokines. Front. Immunol 7, 568. [PubMed: 28018341]

(27). Jorgensen AS, Adogamhe PE, Laufer JM, Legler DF, Veldkamp CT, Rosenkilde MM, and Hjorto GM (2018) CCL19 with CCL21-tail displays enhanced glycosaminoglycan binding with retained chemotactic potency in dendritic cells. J. Leukocyte Biol 104, 401–411. [PubMed: 29768676]

(28). Kiermaier E, Moussion C, Veldkamp CT, Gerardy-Schahn R, de Vries I, Williams LG, Chaffee GR, Phillips AJ, Freiberger F, Imre R, Taleski D, Payne RJ, Braun A, Forster R, Mechtler K,

Muhlenhoff M, Volkman BF, and Sixt M (2016) Polysialylation controls dendritic cell trafficking by regulating chemokine recognition. Science 351, 186–190. [PubMed: 26657283]

(29). Hauser MA, Kindinger I, Laufer JM, Spate AK, Bucher D, Vanes SL, Krueger WA, Wittmann V, and Legler DF (2016) Distinct CCR7 glycosylation pattern shapes receptor signaling and endocytosis to modulate chemotactic responses. J. Leukocyte Biol 99, 993. [PubMed: 26819318]

(30). Hauser MA, Kindinger I, Laufer JM, Spate AK, Bucher D, Vanes SL, Krueger WA, Wittmann V, and Legler DF (2016) Distinct CCR7 glycosylation pattern shapes receptor signaling and endocytosis to modulate chemotactic responses. J. Leukocyte Biol 99, 993–1007. [PubMed: 26819318]

(31). Barmore AJ, Castex SM, Gouletas BA, Griffith AJ, Metz SW, Muelder NG, Populin MJ, Sackett DM, Schuster AM, and Veldkamp CT (2016) Transferring the C-terminus of the chemokine CCL21 to CCL19 confers enhanced heparin binding. Biochem. Biophys. Res. Commun 477, 602–606. [PubMed: 27338641]

(32). Veldkamp CT, Peterson FC, Pelzek AJ, and Volkman BF (2005) The monomer-dimer equilibrium of stromal cell-derived factor-1 (CXCL 12) is altered by pH, phosphate, sulfate, and heparin. Protein Sci. 14, 1071–1081. [PubMed: 15741341]

(33). Thomas MA, He J, Peterson FC, Huppler AR, and Volkman BF (2018) The Solution Structure of CCL28 Reveals Structural Lability that Does Not Constrain Antifungal Activity. J. Mol. Biol 430, 3266–3282. [PubMed: 29913161]

(34). Tyler RC, Wieting JC, Peterson FC, and Volkman BF (2012) Electrostatic optimization of the conformational energy landscape in a metamorphic protein. Biochemistry 51, 9067–9075. [PubMed: 23102260]

(35). Proudfoot AE, Handel TM, Johnson Z, Lau EK, LiWang P, Clark-Lewis I, Borlat F, Wells TN, and Kosco-Vilbois MH (2003) Glycosaminoglycan binding and oligomerization are essential for the in vivo activity of certain chemokines. Proc. Natl. Acad. Sci. U. S. A 100, 1885–1890. [PubMed: 12571364]

(36). Joseph PR, Mosier PD, Desai UR, and Rajarathnam K (2015) Solution NMR characterization of chemokine CXCL8/IL-8 monomer and dimer binding to glycosaminoglycans: structural plasticity mediates differential binding interactions. Biochem. J 472, 121–133. [PubMed: 26371375]

(37). Rey-Gallardo A, Escribano C, Delgado-Martin C, Rodriguez-Fernandez JL, Gerardy-Schahn R, Rutishauser U, Corbi AL, and Vega MA (2010) Polysialylated neuropilin-2 enhances human dendritic cell migration through the basic C-terminal region of CCL21. Glycobiology 20, 1139–1146. [PubMed: 20488940]

(38). Hirose J, Kawashima H, Willis MW, Springer TA, Hasegawa H, Yoshie O, and Miyasaka M (2002) Chondroitin sulfate B exerts its inhibitory effect on secondary lymphoid tissue chemokine (SLC) by binding to the C-terminus of SLC. Biochim. Biophys. Acta, Gen. Subj 1571, 219–224.

(39). Weber M, Hauschild R, Schwarz J, Moussion C, de Vries I, Legler DF, Luther SA, Bollenbach T, and Sixt M (2013) Interstitial dendritic cell guidance by haptotactic chemokine gradients. Science 339, 328–332. [PubMed: 23329049]

(40). Laguri C, Sadir R, Rueda P, Baleux F, Gans P, Arenzana-Seisdedos F, and Lortat-Jacob H (2007) The novel CXCL12gamma isoform encodes an unstructured cationic domain which regulates bioactivity and interaction with both glycosaminoglycans and CXCR4. PLoS One 2, No. e1110. [PubMed: 17971873]

(41). Rueda P, Balabanian K, Lagane B, Staropoli I, Chow K, Levoye A, Laguri C, Sadir R, Delaunay T, Izquierdo E, Pablos JL, Lendinez E, Caruz A, Franco D, Baleux F, Lortat-Jacob H, and Arenzana-Seisdedos F (2008) The CXCL12gamma chemokine displays unprecedented structural and functional properties that make it a paradigm of chemoattractant proteins. PLoS One 3, No. e2543. [PubMed: 18648536]

(42). Vanheule V, Boff D, Mortier A, Janssens R, Petri B, Kolaczkowska E, Kubes P, Berghmans N, Struyf S, Kungl AJ, Teixeira MM, Amaral FA, and Proost P (2017) CXCL9-Derived Peptides Differentially Inhibit Neutrophil Migration In Vivo through Interference with Glycosaminoglycan Interactions. Front. Immunol 8, 530. [PubMed: 28539925]

(43). Vanheule V, Janssens R, Boff D, Kitic N, Berghmans N, Ronsse I, Kungl AJ, Amaral FA, Teixeira MM, Van Damme J, Proost P, and Mortier A (2015) The Positively Charged COOH-

terminal Glycosaminoglycan-binding CXCL9(74–103) Peptide Inhibits CXCL8-induced Neutrophil Extravasation and Monosodium Urate Crystal-induced Gout in Mice. J. Biol. Chem 290, 21292–21304. [PubMed: 26183778]

(44). Egesten A, Eliasson M, Johansson HM, Olin AI, Morgelin M, Mueller A, Pease JE, Frick IM, and Bjorck L (2007) The CXC chemokine MIG/CXCL9 is important in innate immunity against Streptococcus pyogenes. J. Infect. Dis 195, 684–693. [PubMed: 17262710]

(45). Smith EW, Lewandowski EM, Moussouras NA, Kroeck KG, Volkman BF, Veldkamp CT, and Chen Y (2016) Crystallographic Structure of Truncated CCL21 and the Putative Sulfotyrosine-Binding Site. Biochemistry 55, 5746–5753. [PubMed: 27617343]

(46). Jiang LI, Collins J, Davis R, Lin KM, DeCamp D, Roach T, Hsueh R, Rebres RA, Ross EM, Taussig R, Fraser I, and Sternweis PC (2007) Use of a cAMP BRET sensor to characterize a novel regulation of cAMP by the sphingosine 1-phosphate/G13 pathway. J. Biol. Chem 282, 10576–10584. [PubMed: 17283075]

(47). Szpakowska M, Meyrath M, Reynders N, Counson M, Hanson J, Steyaert J, and Chevigne A (2018) Mutational analysis of the extracellular disulphide bridges of the atypical chemokine receptor ACKR3/CXCR7 uncovers multiple binding and activation modes for its chemokine and endogenous non-chemokine agonists. Biochem. Pharmacol 153, 299–309. [PubMed: 29530506]

(48). Szpakowska M, Nevins AM, Meyrath M, Rhainds D, D'Huys T, Guite-Vinet F, Dupuis N, Gauthier PA, Counson M, Kleist A, St-Onge G, Hanson J, Schols D, Volkman BF, Heveker N, and Chevigne A (2018) Different contributions of chemokine N-terminal features attest to a different ligand binding mode and a bias towards activation of ACKR3/CXCR7 compared with CXCR4 and CXCR3. Br. J. Pharmacol 175, 1419–1438. [PubMed: 29272550]

(49). Dixon AS, Schwinn MK, Hall MP, Zimmerman K, Otto P, Lubben TH, Butler BL, Binkowski BF, Machleidt T, Kirkland TA, Wood MG, Eggers CT, Encell LP, and Wood KV (2016) NanoLuc Complementation Reporter Optimized for Accurate Measurement of Protein Interactions in Cells. ACS Chem. Biol 11, 400–408. [PubMed: 26569370]

(50). Veldkamp CT, Koplinski CA, Jensen DR, Peterson FC, Smits KM, Smith BL, Johnson SK, Lettieri C, Buchholz WG, Solheim JC, and Volkman BF (2016) Production of Recombinant Chemokines and Validation of Refolding. Methods Enzymol. 570, 539–565. [PubMed: 26921961]

(51). Moussouras NA, Getschman AE, Lackner ER, Veldkamp CT, Dwinell MB, and Volkman BF (2017) Differences in Sulfotyrosine Binding amongst CXCR1 and CXCR2 Chemokine Ligands. Int. J. Mol. Sci 18, 1894.

(52). Ueno T, Hara K, Willis MS, Malin MA, Hopken UE, Gray DH, Matsushima K, Lipp M, Springer TA, Boyd RL, Yoshie O, and Takahama Y (2002) Role for CCR7 ligands in the emigration of newly generated T lymphocytes from the neonatal thymus. Immunity 16, 205–218. [PubMed: 11869682]

(53). Kuloglu ES, McCaslin DR, Markley JL, and Volkman BF (2002) Structural rearrangement of human lymphotactin, a C chemokine, under physiological solution conditions. J. Biol. Chem 277, 17863–17870. [PubMed: 11889129]

(54). Veldkamp CT, Ziarek JJ, Su J, Basnet H, Lennertz R, Weiner JJ, Peterson FC, Baker JE, and Volkman BF (2009) Monomeric structure of the cardioprotective chemokine SDF-1/CXCL12. Protein Sci. 18, 1359–1369. [PubMed: 19551879]

(55). Kenakin T (2011) Functional selectivity and biased receptor signaling. J. Pharmacol. Exp. Ther 336, 296–302. [PubMed: 21030484]

(56). Drury LJ, Ziarek JJ, Gravel S, Veldkamp CT, Takekoshi T, Hwang ST, Heveker N, Volkman BF, and Dwinell MB (2011) Monomeric and dimeric CXCL12 inhibit metastasis through distinct CXCR4 interactions and signaling pathways. Proc. Natl. Acad. Sci. U. S. A 108, 17655–17660. [PubMed: 21990345]

(57). Roy I, McAllister DM, Gorse E, Dixon K, Piper CT, Zimmerman NP, Getschman AE, Tsai S, Engle DD, Evans DB, Volkman BF, Kalyanaraman B, and Dwinell MB (2015) Pancreatic Cancer Cell Migration and Metastasis Is Regulated by Chemokine-Biased Agonism and Bioenergetic Signaling. Cancer Res. 75, 3529–3542. [PubMed: 26330165]

(58). Getschman AE, Imai Y, Larsen O, Peterson FC, Wu X, Rosenkilde MM, Hwang ST, and Volkman BF (2017) Protein engineering of the chemokine CCL20 prevents psoriasiform

dermatitis in an IL-23-dependent murine model. Proc. Natl. Acad. Sci. U. S. A 114, 12460–12465. [PubMed: 29109267]

(59). Ziarek JJ, Kleist AB, London N, Raveh B, Montpas N, Bonneterre J, St-Onge G, DiCosmo-Ponticello CJ, Koplinski CA, Roy I, Stephens B, Thelen S, Veldkamp CT, Coffman FD, Cohen MC, Dwinell MB, Thelen M, Peterson FC, Heveker N, and Volkman BF (2017) Structural basis for chemokine recognition by a G protein-coupled receptor and implications for receptor activation. Sci. Signaling 10, 10.

(60). Rollins BJ (1997) Chemokines. Blood 90, 909–928. [PubMed: 9242519]

(61). Jorgensen AS, Larsen O, Uetz-Von Allmen E, Luckmann M, Legler DF, Frimurer TM, Veldkamp CT, Hjorto GM, and Rosenkilde MM (2019) Biased Signaling of CCL21 and CCL19 Does Not Rely on N-Terminal Differences, but Markedly on the Chemokine Core Domains and Extracellular Loop 2 of CCR7. Front. Immunol 10, 2156. [PubMed: 31572374]

(62). Kohout TA, Nicholas SL, Perry SJ, Reinhart G, Junger S, and Struthers RS (2004) Differential desensitization, receptor phosphorylation, beta-arrestin recruitment, and ERK1/2 activation by the two endogenous ligands for the CC chemokine receptor 7. J. Biol. Chem 279, 23214–23222. [PubMed: 15054093]

(63). Inoue A, Raimondi F, Kadji FMN, Singh G, Kishi T, Uwamizu A, Ono Y, Shinjo Y, Ishida S, Arang N, Kawakami K, Gutkind JS, Aoki J, and Russell RB (2019) Illuminating G-Protein-Coupling Selectivity of GPCRs. Cell 177, 1933–1947. [PubMed: 31160049]

(64). Stein JV, Rot A, Luo Y, Narasimhaswamy M, Nakano H, Gunn MD, Matsuzawa A, Quackenbush EJ, Dorf ME, and von Andrian UH (2000) The Cc Chemokine Thymus-Derived Chemotactic Agent 4 (Tca-4, Secondary Lymphoid Tissue Chemokine, 6ckine, Exodus-2) Triggers Lymphocyte Function–Associated Antigen 1–Mediated Arrest of Rolling T Lymphocytes in Peripheral Lymph Node High Endothelial Venules. J. Exp. Med 191, 61–76. [PubMed: 10620605]

(65). Phillips AJ, Taleski D, Koplinski CA, Getschman AE, Moussouras NA, Richard AM, Peterson FC, Dwinell MB, Volkman BF, Payne RJ, and Veldkamp CT (2017) CCR7 Sulfotyrosine Enhances CCL21 Binding. Int. J. Mol. Sci 18, 1857.

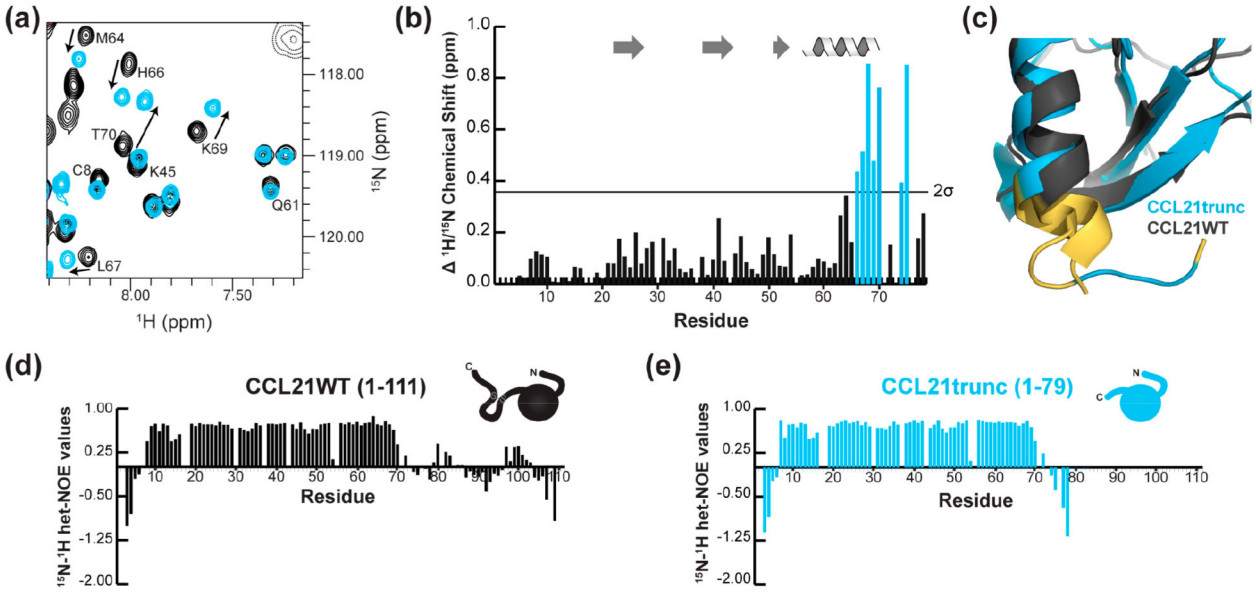

Figure 1.

CCL21WT and CCL21trunc exhibit structural differences. (a) ^{15}N–^{1}H HSQC overlays of CCL21WT (black) and CCL21trunc (blue) at 700 μM. Arrows highlight the differences between the two spectra. (b) Combined ^{1}H/^{15}N chemical shift perturbations (CSP) plotted per each residue. Prolines (residues 18, 30, 37, 43, 55, 71, 73, 76) and residues not observed in the HSQC (S1, D2, I17, R84) were given a value of 0. Residues with a combined CSP greater than two standard deviations (2σ) above the baseline are highlighted in light blue. (c) Alignment of the solved NMR solution structure of CCL21WT (PDB ID: 2L4N, black) with the crystal structure of CCL21trunc (PDB ID: 5EKI, light blue). Large CSPs > 1σ from the baseline from panel b are highlighted in the inset in yellow. The residues highlighted in yellow correspond to differences between the two structures, notably at the end of the helix. (d, e) ^{15}N–^{1}H heteronuclear NOE values plotted per residue for CCL21WT (black) and CCL21trunc (light blue) at 700 μM. The negative values indicate N- and C-termini of the chemokines are flexible. The C-terminal disulfide bond (residues 80–99) adds some stability (positive het-NOE values) to the otherwise flexible C-terminus for CCL21WT.

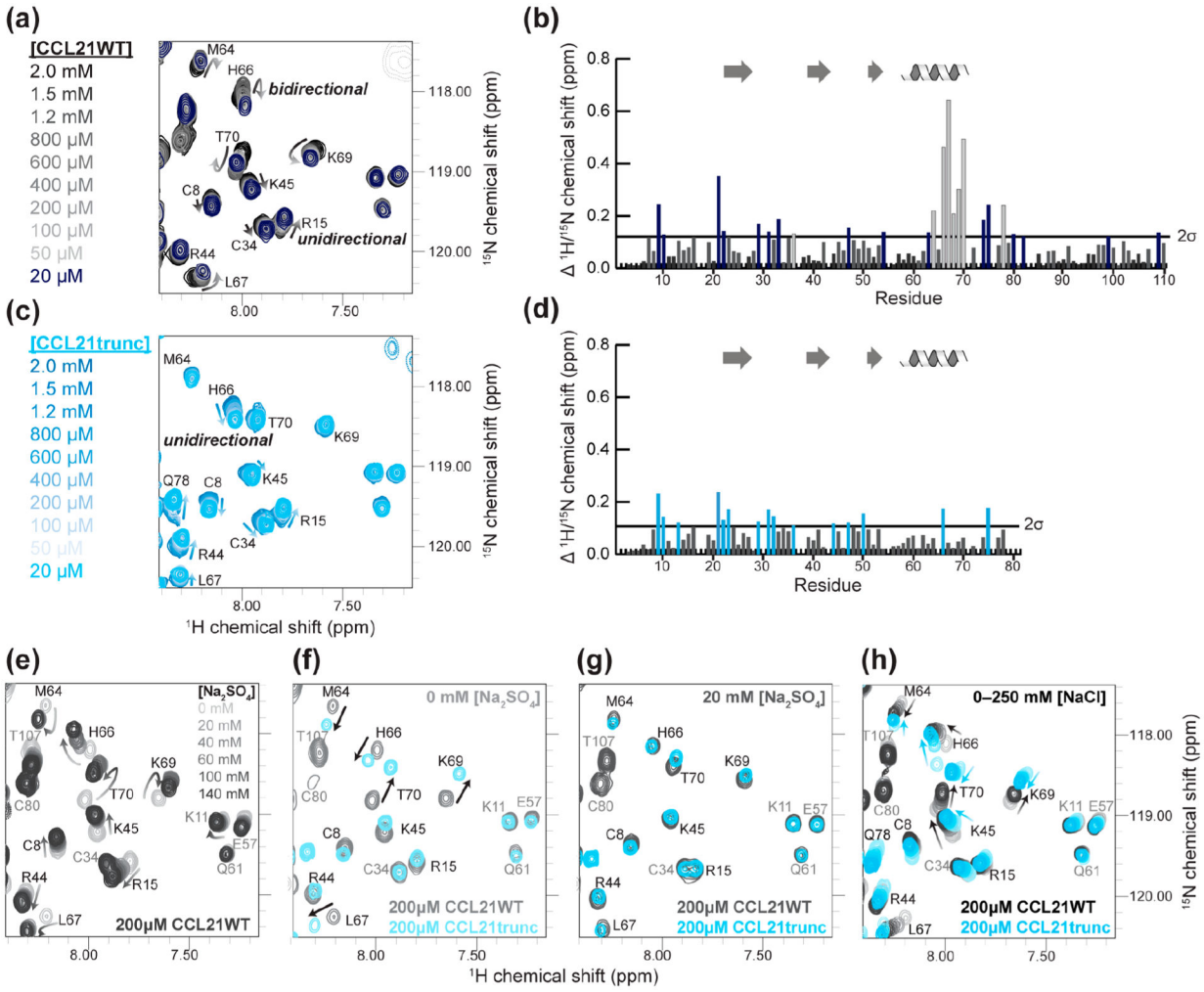

Figure 2.

CCL21WT and CCL21trunc undergo a monomer–dimer equilibrium. (a) ^{15}N–^{1}H HSQC spectra of CCL21WT at 2 mM, 1.5 mM, 1.2 mM, 800 μM, 600 μM, 400 μM, 200 μM, 100 μM, 50 μM, and 20 μM. (b) Concentration-dependent chemical shift perturbations for CCL21WT. Residues highlighted in purple had combined $^{1}H/^{15}N$ chemical shift perturbations greater than 2 standard deviations (2σ) from the baseline. Residues highlighted in gray have bidirectional peak movement. (c) ^{15}N–^{1}H HSQC spectra of CCL21trunc at 2 mM, 1.5 mM, 1.2 mM, 800 μM, 600 μM, 400 μM, 200 μM, 100 μM, 50 μM, and 20 μM. (d) Concentration-dependent chemical shift perturbations for CCL21trunc. Residues highlighted blue had combined $^{1}H/^{15}N$ chemical shift perturbations greater than 2 standard deviations (2σ) from the baseline. (e) ^{15}N–^{1}H HSQC spectra of CCL21WT (200 μM) in increasing concentrations of Na_2SO_4 (0–140 mM) reveal chemical shift perturbations that largely reverse the pattern observed upon dilution of CCL21WT from panel a. (f) HSQC overlay of 200 μM CCL21WT and CCL21trunc in 0 mM Na_2SO_4 illustrates truncation-dependent shift differences. (g) HSQC overlay of 200 μM CCL21WT and CCL21trunc in 20 mM Na_2SO_4 shows that shift differences associated with the CCL21 C-terminus disappear with the first addition of Na_2SO_4. (h) ^{15}N–^{1}H HSQC spectra of 200 μM CCL21WT and CCL21trunc in

increasing concentrations of NaCl (0–250 mM) reveal that peaks for residues, which are separated in the spectra for CCL21WT and CCL21trunc shown in panel g, converge on a new position in response to the addition of NaCl.

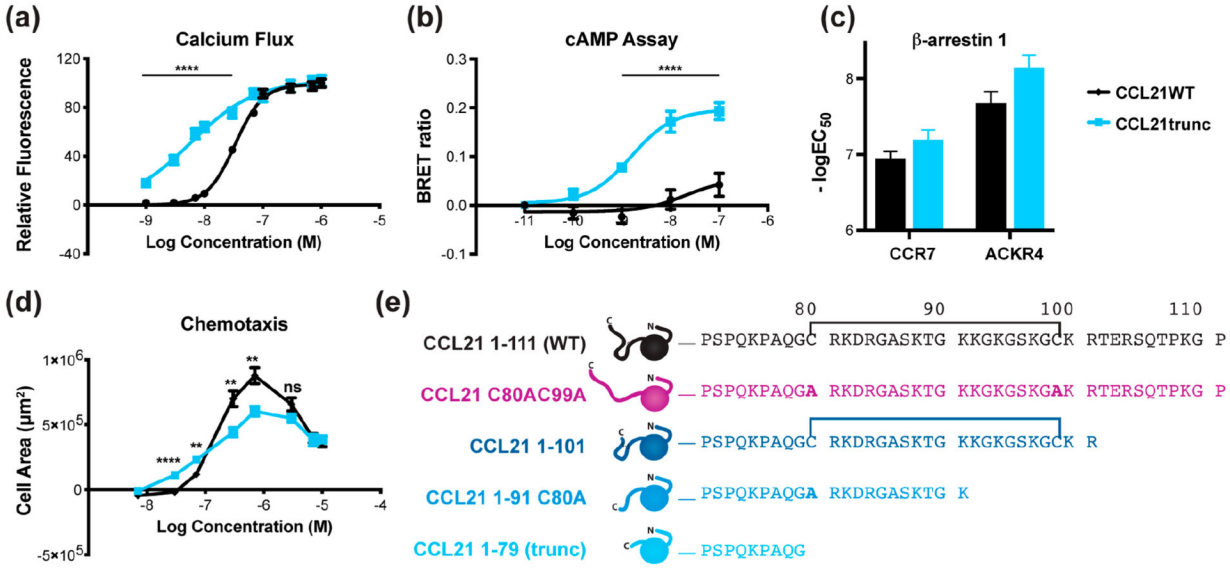

Figure 3.

CCL21WT and CCL21trunc exhibit functional differences. (a) Dose–response curves for calcium mobilization induced in CHEM-1 CCR7$^+$ cells for CCL21WT (black, EC_{50} = 33.4 nM ± 1.1, n = 11) and CCL21trunc (light blue, EC_{50} = 5.85 nM ± 1.2, n = 5). Curves were normalized to the maximum CCL21WT response. (b) Cyclic AMP (cAMP) inhibition was tested via BRET in CHO cells transiently transfected with CCR7 and the cAMP sensor Camyel. EC_{50} values were 20.2 nM and 1.6 nM for CCL21WT and CCL21trunc, respectively (n = 5). (c) Recruitment of β-arrestin 1 to either CCR7 or ACKR4. Potencies are shown as $-\log EC_{50}$, where $\log EC_{50}$ and standard error values were obtained by nonlinear fitting of the BRET intensity as a function of CCL21WT or CCL21trunc concentration. (d) Chemotaxis was measured via the IncuCyte live-cell imaging platform and quantified by the area covered by migrated cells. B16/F1 melanoma cells transduced with CCR7 showed that CCL21trunc was more potent, while CCL21WT was more effective at higher concentrations (n = 4–6). Statistical significance was determined with an unpaired t-test. $^{**}P < 0.01$, $^{****}P < 0.0001$, ns = not significant. Values are mean ± SEM. Design of CCL21 variants used in this study. (e) Design of mutants to probe the role of the extended CCL21 C-terminus.

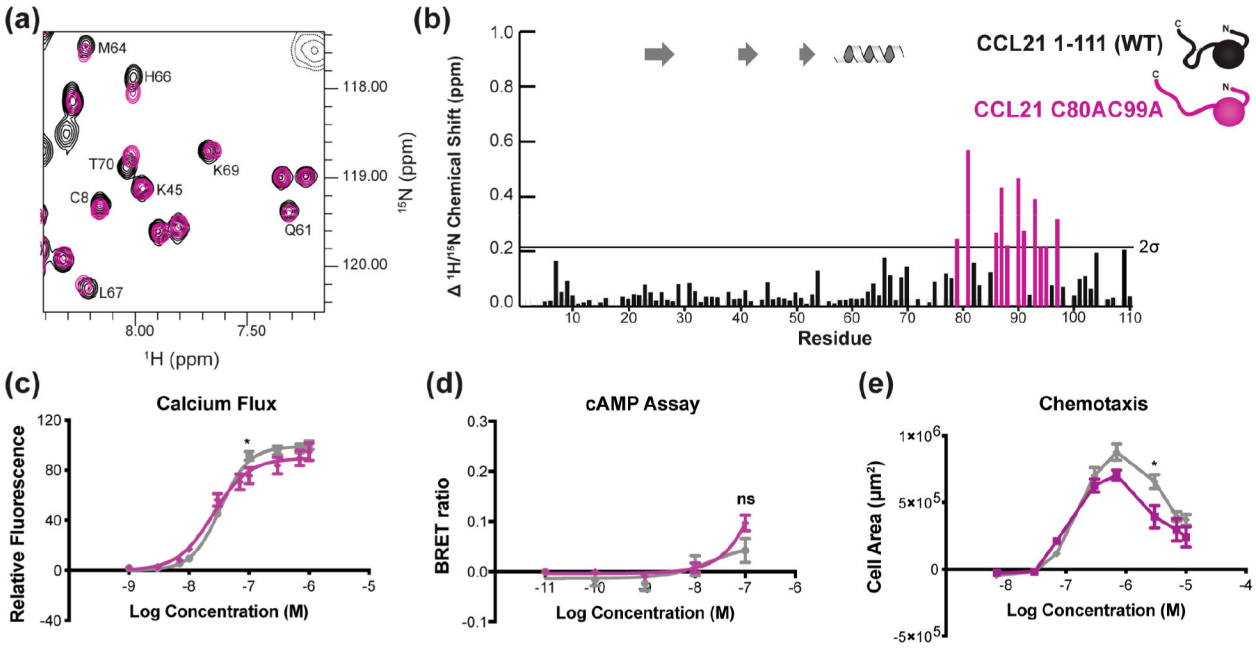

Figure 4.

Elimination of the C-terminal disulfide bond does not recapitulate CCL21trunc features. (a) ^{15}N–^{1}H HSQC overlays of CCL21WT (black) and CCL21 C80AC99A (magenta) at 700 μM. The full differences are quantified in panel b in the combined chemical shift perturbation (CSP) plot. Residues with CSP two standard deviations (2σ) above the baseline are highlighted in magenta. Importantly, these residues reside within the loop region previously formed by the third disulfide bond, which is absent in this variant. (c) Dose–response curves for calcium mobilization induced in CHEM-1 CCR7^{+} cells for CCL21C80AC99A (magenta, EC_{50} = 25.3 nM, n = 6) compared to CCL21WT (gray). Curves were normalized to the maximum CCL21WT response. (d) BRET assay demonstrating cAMP inhibition (n = 5). (e) Chemotaxis measured via IncuCyte in B16/F1 cells transduced with CCR7. Chemotaxis was quantified as the area covered by migrated cells and revealed little difference at key low concentrations, nor at the peak migration point. CCL21WT was more effective at 3 μM. Statistical significance for panels c, d, and e was determined with an unpaired t-test. *$P < 0.05$, ns = not significant. Values are mean ± SEM.

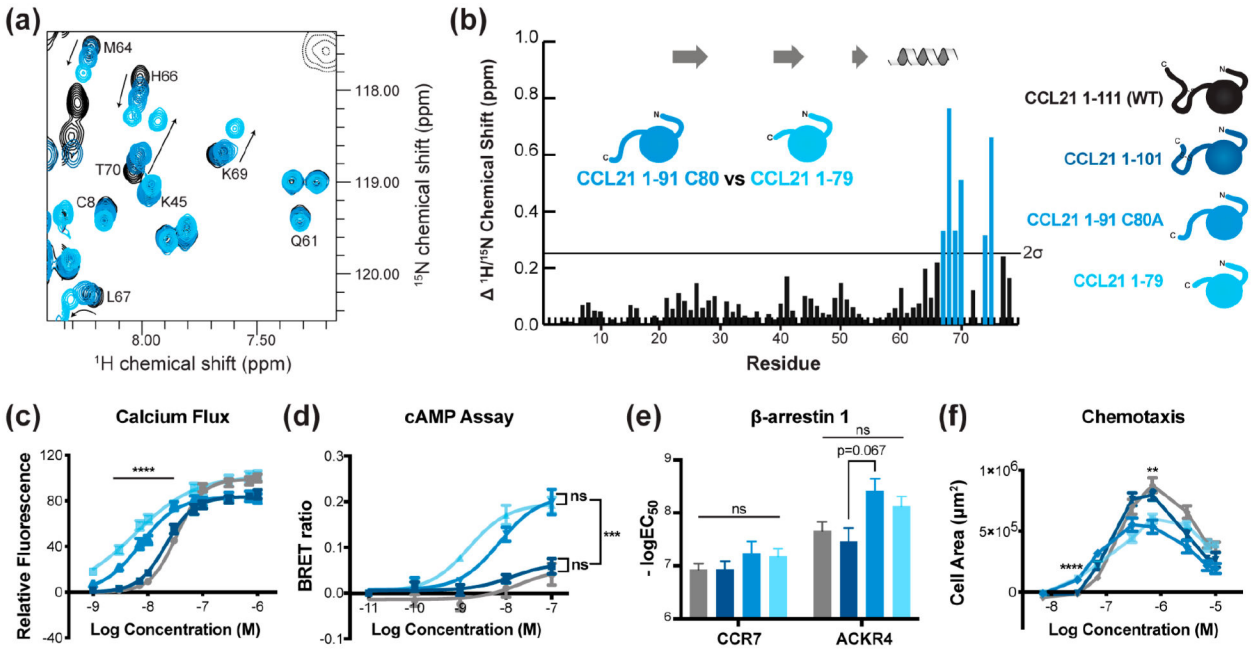

Figure 5.

C-Terminal truncation variants focus on the region responsible for the CCL21WT and CCL21trunc structural and functional profiles. (a) ^{15}N–^{1}H HSQC overlays of each of the CCL21 variants at 700 μM. Arrows highlight large differences in chemical shifts. The largest global difference in peak position occurs with the final truncation. The CCL21 1–91C80A, CCL21 1–101, CCL21 C80AC99A, and CCL21WT HSQCs overlap well, while the CCL21trunc spectrum is different, suggesting residues 80–90 are responsible for maintaining the differences in the HSQC (see Figure S5). The difference between the CCL21trunc and CCL21 1–91C80A spectra are quantified in the CSP plot shown in panel b. This plot corresponds well with Figure 1b, indicating the difference between CCL21WT and CCL21trunc is nearly identical to the difference between CCL21 1–91C80A and CCL21trunc. Functional assays of CCL21 C-terminal truncation variants reveal two different profiles grouped between the two shorter and two longer CCL21 mutants. (c) Calcium flux assays in CHEM-1 CCR7+ cells testing the dose response of CCL21 variants (EC_{50} CCL21 1–91C80A = 7.30 nM ± 1.1, n = 5, CCL21 1–101 = 21.45 nM ± 1.1, n = 6). Curves were normalized to the maximum CCL21WT response. (d) cAMP inhibition assays reveal a grouping between CCL21trunc and CCL21 1–91C80A, and the longer CCL21 1–101 and CCL21WT variants (n = 5). (e) Recruitment of β-arrestin 1 to either CCR7 or ACKR4. Potencies are shown as $logEC_{50}$, where $logEC_{50}$ and standard error values were obtained by nonlinear fitting of the BRET intensity as a function of CCL21WT or CCL21trunc concentration. (f) Chemotaxis in B16/F1 melanoma cells transduced with CCR7 showed that CCL21trunc and CCL21 1–91C80A were more potent, while CCL21 1–101 and CCL21WT were more effective at higher concentrations (n = 4–6). Statistical significance for panels c, d, e, and f was determined with a one-way ANOVA. ** $P < 0.01$, *** $P < 0.001$, **** $P < 0.0001$, ns = not significant. Values are mean ± SEM.

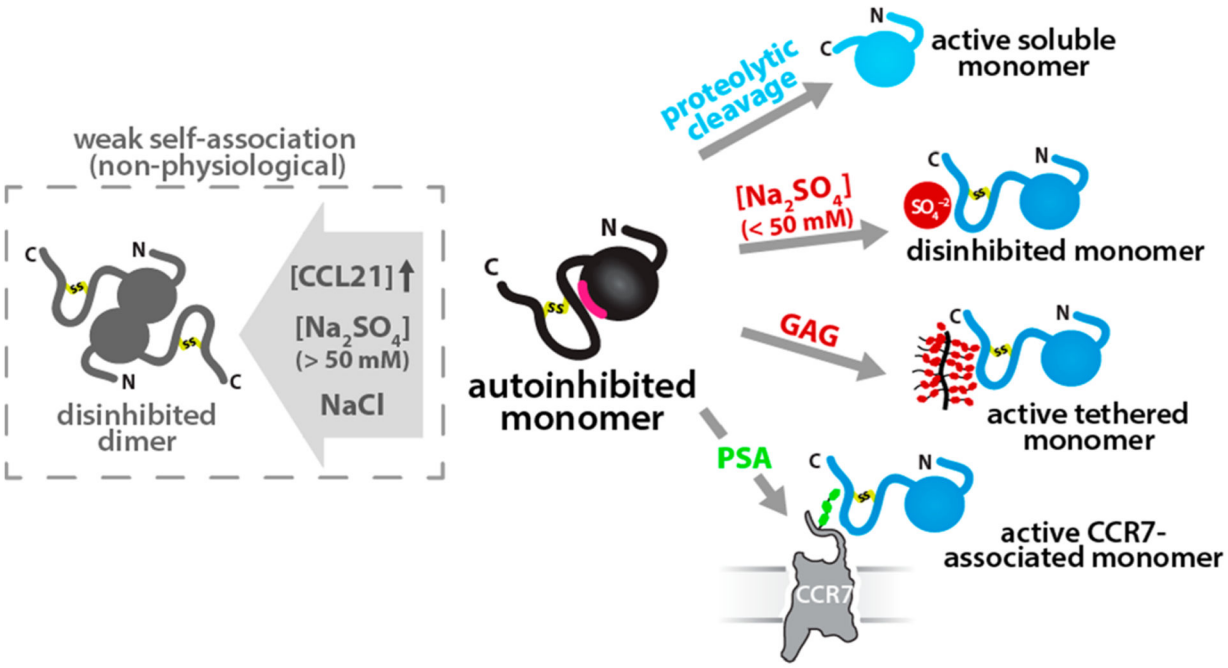

Figure 6.

Disruption of intramolecular CCL21 contacts. Accessible conformational states of CCL21 are depicted schematically based on NMR chemical shift perturbations from this work and published studies. At physiologically relevant nM–μM concentrations in the absence of other binding partners, CCL21 exists in an autoinhibited monomeric state (black) characterized by weak interactions between the flexible C-terminal domain (residues 80–90) and the folded chemokine domain (including residues at the end of the α-helix; magenta). Cleavage of the C-terminal tail by DC proteases or other extracellular enzymes produces an active, soluble CCL21. The addition of 20 mM Na_2SO_4 induces shift perturbations that mimic truncation, consistent with disruption of autoinhibitory contacts. Binding of a heparin disaccharide, PSA, or a CCR7 N-terminal peptide has comparable effects on the NMR spectrum. We speculate that CCL21 engagement with extracellular matrix GAGs or its post-translationally modified GPCR ensures the chemokine domain is in an active conformation. Supraphysiological CCL21 concentrations (>200 μM) or high salt concentrations promote CCL21 self-association with little if any impact on chemokine function.